RESEARCH ARTICLE | FEBRUARY 15 2022

Interfacial dynamics in inverted-headgroup lipid membranes

Special Collection: Time-resolved Vibrational Spectroscopy

Euihyun Lee ; Xiao You ; Carlos R. Baiz

J. Chem. Phys. 156, 075102 (2022)
https://doi.org/10.1063/5.0080153

The Journal of Chemical Physics ARTICLE scitation.org/journal/jcp

Interfacial dynamics in inverted-headgroup lipid membranes

Cite as: J. Chem. Phys. 156, 075102 (2022); doi: 10.1063/5.0080153
Submitted: 29 November 2021 • Accepted: 25 January 2022 •
Published Online: 15 February 2022

Euihyun Lee, Xiao You, and Carlos R. Baiz[a)]

AFFILIATIONS

Department of Chemistry, The University of Texas at Austin, Austin, Texas 78712, USA

Note: This paper is part of the JCP Special Topic on Time-Resolved Vibrational Spectroscopy.
[a)]**Author to whom correspondence should be addressed:** cbaiz@cm.utexas.edu

ABSTRACT

Inverted-headgroup (choline-phosphate) lipids are synthetic lipids that are not found in nature and are used as model systems to understand the role of headgroup dipole orientation. Recently, studies revealed that the net orientation of interfacial water strongly depends on the headgroup electrostatics, i.e., the charges and dipole generated by the phosphate and the choline groups. In order to characterize interfacial H-bond dynamics, we measured two-dimensional infrared spectra of the ester carbonyl band and performed molecular dynamics simulations in fully hydrated 1,2-dioleoyl-sn-glycero-3-phosphocholine and 2-((2,3-bis(oleoyloxy)propyl)-dimethyl-ammonio)ethyl ethyl phosphate (DOCPe) lipid bilayers. The experiments and simulations suggest that the reverse dipole generated by the inverted-headgroup in DOCPe does not affect the carbonyl H-bond populations or the interfacial water H-bond dynamics. However, while phosphate-associated waters in both lipids appear to show a similar H-bond structure, carbonyl-associated waters are characterized by a slightly disrupted H-bond structure in the DOCPe bilayer, especially within the second hydration shell. Our findings show that changes in net water orientation perturb the water H-bonds at the linker region between the headgroup and the lipid tail, although this perturbation is weak.

I. INTRODUCTION

Cell membranes are host to a large array of proteins, and several biochemical processes take place within the interfacial environments at the membrane/water region.[1,2] Heterogeneity, compartmentalization, and asymmetry can significantly affect these interfacial environments, but the role that these environments play in mediating biochemical processes remains largely unknown. Model lipid membranes are often used for biophysical studies, specifically zwitterionic phosphatidylcholine (PC) lipids, containing a hydrocarbon tail linked to a negatively charged phosphate group via an ester linkage and capped by a positively charged choline group. These lipids have been the subject of countless experimental and computational studies aimed at investigating the dynamics, structure, and interactions of lipids and interfacial water.[3–25]

In cell membranes, lipid composition is intimately linked to the structure and the function of membrane proteins.[26] In addition, part of these effects may be linked to the net orientation of the water molecules induced by the headgroup electrostatics. For example, zwitterionic lipids have weaker interfacial water orienting ability than anionic lipids.[27] Recently, the role of the headgroup dipole on interfacial properties has begun to be studied more systematically using inverted-headgroup analogs of phosphatidylcholine (PC), the so-called "CP" lipids.[24,25] This inverted-headgroup lipid is a synthetic artificial lipid that is not found in nature.[28] Both lipids have an ~20 D permanent dipole but with opposite orientation, and bilayers can produce large interfacial electric fields of 10^8–10^9 V/m, orienting water molecules at the interface.[29] The correlation between water orientation and H-bond dynamics is still unclear, requiring studies focused on characterizing waters located within specific regions of the interface, including choline, phosphate, and carbonyl groups.[25]

Here, we investigate the interfacial water H-bonding structure and dynamics in both "PC" and "CP" lipids [Figs. 1(a) and S1(a)], namely, 1,2-dioleoyl-sn-glycero-3-phosphocholine (DOPC) and 2-((2,3-bis(oleoyloxy)propyl)-dimethyl-ammonio)ethyl ethyl phosphate (DOCPe), respectively, to elucidate the effects of water orientation on the linker region, i.e., ester carbonyl groups. In brief, we measured the ester carbonyl dynamics using ultrafast two-dimensional infrared (2D IR) spectroscopy and interpreted the measurements using molecular dynamics (MD) simulations. Near-quantitative agreement between experimental and computational results suggests that simulations provide an atomistic level of the

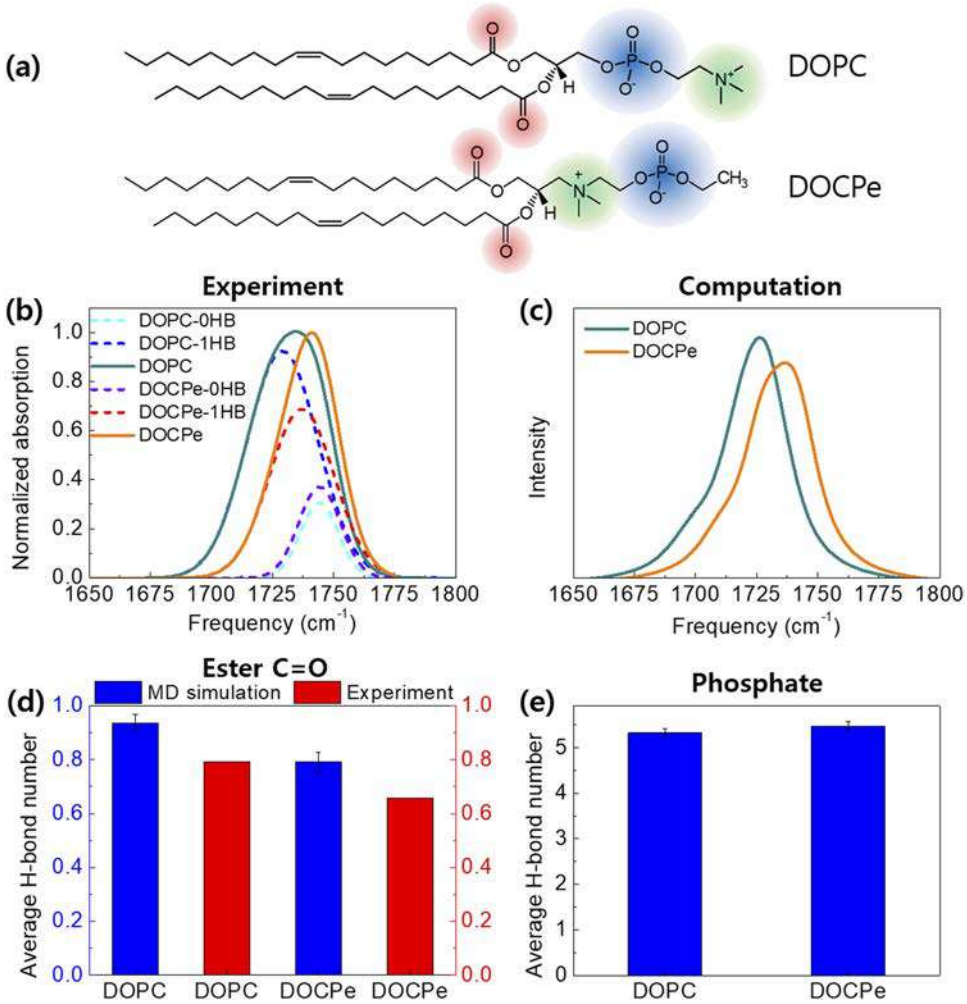

FIG. 1. (a) Structures of DOPC and DOCPe lipids. (b) Absorption spectra of DOPC and DOCPe lipid carbonyls (solid lines) and their two Gaussian-fitted lines (dashed lines). (c) Computed IR spectra of DOPC and DOCPe lipid carbonyls from electronic structure calculations. (d) Average H-bond number between the lipid carbonyl group and water obtained from MD simulations and experiments (b). (e) Average H-bond number between the lipid phosphate group and water obtained from MD simulations.

description of headgroup effects on the interfacial H-bond structure and dynamics.

II. METHODS

A. Experimental methods

1. Sample preparation

DOPC and DOCPe vesicles were prepared as described previously.[30] In brief, DOPC and DOCPe 25 mg/ml chloroform solutions were purchased from Avanti Polar Lipids (Birmingham, AL), stored at −25 °C, and used without further purification. Chloroform was fully evaporated before bypassing a dry nitrogen stream followed by desiccation under a mild vacuum. Lipids were then reconstituted in D_2O to a concentration of 50 mg/ml. Reconstituted samples were subject to six freeze–thaw cycles, 20-min sonication, and extrusion through 100-nm-pore filters at 60 °C to obtain uniform 100-nm vesicles.

2. Infrared absorption spectroscopy

Absorption spectra were recorded on a Bruker Vertex 70 spectrometer as described previously.[30] The spectrometer and sample chamber were purged with dry air to minimize the absorption from water vapor. Samples were held between two 1-mm CaF_2 windows separated by a 25-μm polytetrafluoroethylene (PTFE) spacer in a brass sample cell. All spectra were measured at 25 °C, well above the gel to the liquid phase transition temperature of the lipids.

3. Ultrafast 2D IR spectroscopy

Ultrafast 2D IR spectra were measured using a pulse-shaper-based 2D IR spectrometer described previously.[31] In brief, 2D IR

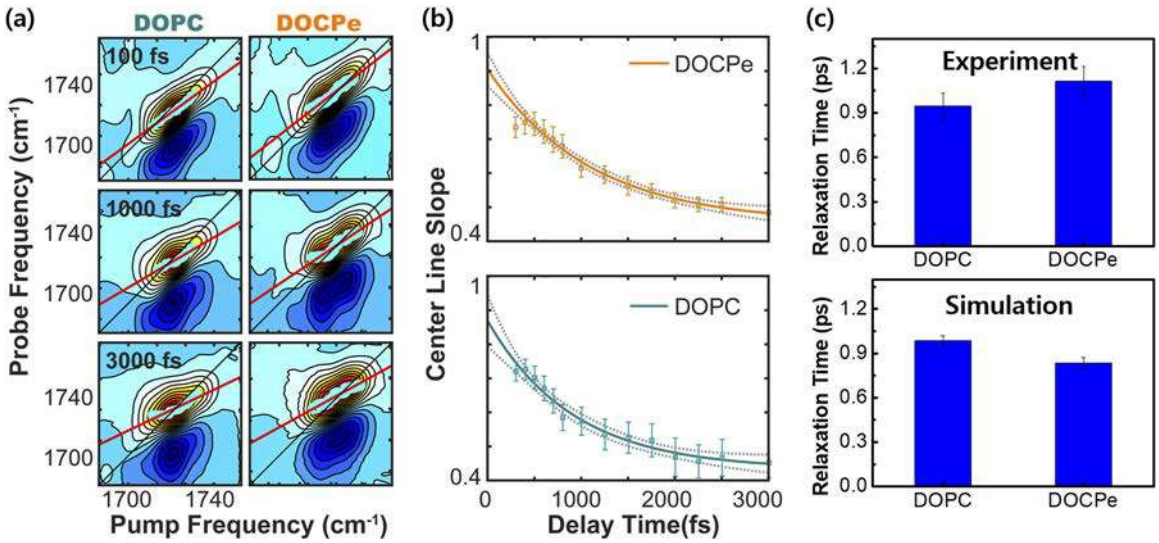

FIG. 2. (a) Experimental 2D IR spectra of the DOPC and DOCPe carbonyl stretching modes at three waiting times to show the decrease in diagonal elongation. (b) Center line slope decays of DOPC and DOCPe extracted from 2D IR spectra along with single-exponential fits. (c) Single exponential decay constants extracted from fits to the experimentally measured CLS decay and decay constants extracted from frequency–frequency correlation functions obtained from MD simulation trajectories.

measurements consist of excitation pulses (pump) and a detection pulse (probe) resonant with the carbonyl stretching mode. 2D IR spectra show the characteristic positive–negative peak doublet that arises from the ground-state bleach (red contours, diagonal) and excited-state absorption contributions (blue contours, below-diagonal) as shown in Fig. 2(a). Initially, the peaks are diagonally elongated, indicating that the pump and probe frequencies are correlated. This correlation between the pump and the probe decreases over time as a result of spectral diffusion. A center line slope (CLS) analysis is used to quantify the diagonal elongation.[32] The time evolution of the CLS as a function of waiting time, t_2 [Fig. 2(b)], represents the frequency–frequency correlation function of the carbonyls.

Pump and probe pulses were centered near 1700 cm^{-1}. Coherence times (t_1) were scanned up to 3 ps in 20 fs steps. Spectra were measured at a series of waiting times, t_2, from 50 to 3000 fs. The pump and probe pulses were maintained at perpendicular polarizations to reduce pump scatter. The experimental temperature was set to 30 °C to maintain the DOPC and DOCPe lipids well above their phase transition temperature. The CLS was extracted by mapping the probe frequency, ω_3, at each pump frequency, ω_1, corresponding to the maximum position of the positive peaks. The resulting scatter plots are fit to a line, and the slope is extracted from each fit. The decay constants and offsets were obtained from fitting the decay curve to a single exponential function.

B. Molecular dynamics simulations

Simulations were performed using the GROMACS 2019.4 simulation package[33] and the CHARMM36 general force field.[34] The initial DOPC lipid bilayer configuration was constructed using the Chemistry at Harvard Molecular Mechanics (CHARMM)-graphical user interface (GUI) membrane builder tool.[35–38] However, no force fields exist for the DOCPe lipid in the CHARMM-GUI membrane builder, and we built the DOCPe force fields based on the general CHARMM force field. Lipid bilayer structures were solvated by water molecules using the Packmol package.[39] Here, simulation boxes consist of 100 lipids and 5000 water molecules (i.e., lipid:water = 1:50, fully hydration). The TIP4Pew water model was used for all simulations.[40] A cutoff distance of 12 Å for the Lennard-Jones interaction and the real space part of the Ewald sum were used, and the particle mesh Ewald (PME) method[41] was applied for long-range electrostatic interactions.

Initial bilayer configurations were energy-minimized for 10 000 steps and then a 10-ns NPT equilibration was performed with strong positional restraints (1000 kJ mol^{-1} nm^{-2}) on the lipid atoms to equilibrate water distributions around the lipid bilayer surface. Next, a 10-ns NVT equilibration was performed using the V-rescale thermostat at 303 K, followed by a 100-ns NPT equilibration to obtain a properly equilibrated box density. After the area-per-lipid stabilized [Figs. S1(b) and S1(c)], the NPT production simulations were performed using a Nose–Hoover thermostat and a Parrinello–Raman barostat. Depending on the purpose of the analysis, two different-length production simulations were carried out. First, to study the carbonyl frequency fluctuation dynamics, 500 ps trajectories with snapshots were saved every 20 fs. Second, to characterize the statistical water distributions, 10 ns trajectories were carried out with snapshots stored every 1 ps. Hydrogen-bond populations were computed using geometric criteria described previously.[18,42,43] Briefly, a donor–acceptor (D-A) cutoff distance of 0.35 nm and an H-D-A angle of 30° were used to define an H-bonds involving the ester carbonyl or phosphate oxygen atoms. Frequency fluctuations of the carbonyls were computed using an electrostatic map described previously.[44] The interfacial water region was defined as the region between 1 and 2 nm from the bilayer center (Fig. S1). This region was used for mean-squared displacement and orientational relaxation analyses reported in Fig. S3.

C. Electronic structure models

The vibrational frequencies of the carbonyl groups were computed at the B3LYP/6-31+G(d) level of theory, using 15 different DOPC and DOCPe configurations randomly sampled from the MD trajectories, to understand the impact of the chemical differences between DOPC and DOCPe lipids on the vibrational mode frequencies of the carbonyl groups.[45] We removed lipid tails to exclude potential effects of the tail orientation, as shown in Fig. S2. Vibrational frequencies and transition dipole moments extracted from harmonic frequency calculations were convolved with a Gaussian function to generate the spectra shown in Fig. 1(c). A frequency scaling factor of 0.9614[46,47] was applied to match with the experimental spectrum.

III. RESULTS

A. Carbonyl/phosphate H-bond populations

Since the carbonyl spectra reflect H-bond environments involving local water molecules,[48] measuring H-bond populations are the first step to understanding headgroup effects on interfacial waters. Carbonyl H-bond populations are extracted directly from the IR absorption lineshapes. Spectra can be decomposed into the 0 and 1 H-bond ensemble peaks by fitting the band to a combination of two Gaussian functions. Populations are proportional to the peak areas weighted the ratio of the oscillator strength, as previously reported ($\varepsilon_{1HB}/\varepsilon_{0HB} = 1.49$).[19]

The DOPC spectrum shows broader line shapes compared to DOCPe [Fig. 1(b)], indicating that DOPC lipid carbonyl groups experience a more heterogeneous environment compared to DOCPe. In addition, there is an overall shift in the peaks between the two lipids. DOPC peaks are red-shifted compared to DOCPe. Normal mode calculations using density functional theory (DFT) were performed using isolated DOPC and DOCPe lipids, respectively, to explain the observed frequency differences. Similar ~20 cm^{-1} frequency shifts between the carbonyls in the two lipids were observed in the normal mode analysis, which shows that DOPC carbonyl appears at a slightly lower frequency compared to DOCPe, as shown in Fig. 1(c). This shows that the frequency shifts dominantly originate from the chemical differences between the two species not from the environments. The DOPC absorption band is also broader than DOCPe, which can be attributed to the larger frequency shift between the 0 and 1 HB peaks in DOPC as well as a larger 1 HB population (Table S1). The 1 HB peak has a larger width compared to the 0 HB and, as such, can contribute to an increase in the overall width of the band.

The FTIR spectra show that the 1 H-bond peak [dashed lines in Fig. 1(b)] in DOPC has a larger peak area compared to DOCPe, indicating increased hydrogen bonding for DOPC. The H-bond populations extracted from FTIR lineshapes are directly compared to the average H-bond populations from the MD trajectories [Fig. 1(d)]. Here, the average H-bond numbers from the experiment were extracted by the oscillator-strength-weighted areas of the two peaks [Fig. 1(b)].[19] In both experiment and simulation, we found out that DOCPe exhibits fewer H-bonds with water compared to the DOPC lipid (0.94 → 0.79 in simulation and 0.79 → 0.66 in the experiment). Interestingly, computed H-bond numbers between the phosphate group and water in both systems did not show any differences [Fig. 1(e)]. This means that the inverted-headgroup effect does not change the H-bond in the group in the headgroup region but does perturb the linker region, although this perturbation is small.

B. Lipid carbonyl dynamics

The frequency fluctuations report on the local C=O group H-bond dynamics.[18,19] To investigate inverted-headgroup effects on dynamics, we measured the frequency fluctuation correlation times of ester C=O stretching modes. Since the carbonyl frequencies are sensitive to the H-bond environment, the 2D IR measurements directly report on the interfacial water dynamics. Specifically, the diagonal elongation of the 2D IR lineshapes is quantified through a center line slope analysis, and the loss in frequency correlation as a function of waiting time is fit to an exponential [Figs. 2(a) and 2(b)]. The relaxation time constants for DOPC and DOCPe lipid carbonyl stretching offer a direct comparison of dynamics for the two species [Fig. 2(c), top]. Despite the different water orientations supported by the two lipids, the dynamics are indistinguishable within measurement error (0.95 ± 0.08 ps for DOPC and 1.1 ± 0.10 ps for DOCPe). This means that the inverted-headgroup and its different water orientations do not impact the carbonyl dynamics within the headgroup region. Next, we examine these effects in more detail through MD simulations.

The MD trajectories offer an atomistic view of the local water dynamics in DOPC and DOCPe. Computationally, a C=O frequency correlation function (FFCF) can be directly compared to the CLS relaxation, as described previously.[44] The relaxation times shown in Fig. 2(c), bottom, are in good agreement with experiments, both exhibiting a ~1 ps decay time. Furthermore, both species, DOPC and DOCPe, show nearly identical dynamics (0.99 ± 0.03 and 0.84 ± 0.04 ps relaxation times, respectively). Even though there is a difference in the relative order of the experimental and simulated FFCF, decay time constants and the values in both experiment and simulation are very similar; in fact, the measured values are indistinguishable within experimental error. Thus, both experiments and simulations suggest that the inverted-headgroup does not alter water dynamics within the linker region. One important consideration is the large differences in area-per-lipid between the two systems. The simulated area-per-lipid values of DOPC and DOCPe are 67.6 and 77.6 $Å^2$, respectively, which are in good agreement with the experiment.[25] To examine the relation between area-per-lipid and dynamics, we carried out a separate set of MD simulations at a lateral pressure of 5 bars (Fig. S3), with the purpose of reducing the area-per-lipid. We observed that the DOPC area-per-lipid at 5 bars is reduced by only 3 $Å^2$ compared to original MD trajectories at 1 bar, and DOCPe area-per-lipid remains unchanged. The FFFC decay constants in both systems at 1 and 5 bars are indistinguishable, indicating small changes in area-per-lipid do not have an effect on the local water dynamics, as measured through the carbonyl vibration.

C. H-bond structure of carbonyl- and phosphate-associated water

Radial distribution functions (RDFs) and orientational distribution functions (ODFs) of waters around phosphate and carbonyl groups were computed using the phosphate or the carbonyl oxygen atoms as a reference. The RDFs of phosphate-associated water

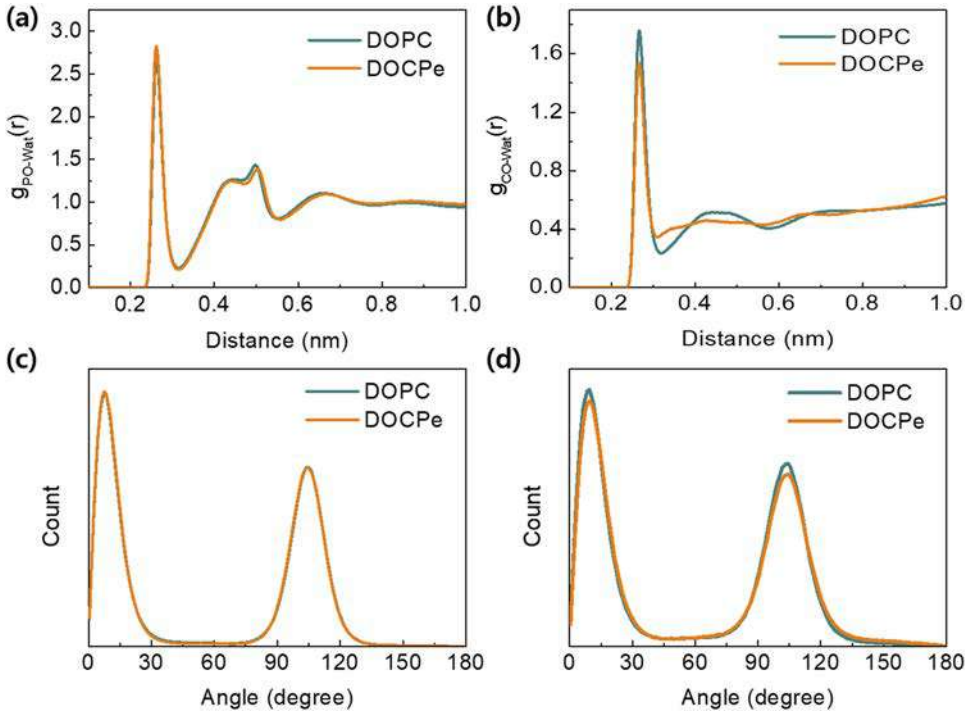

FIG. 3. (a) and (b) Computed RDFs between phosphate oxygen and water oxygens (a) and between carbonyl oxygens and water oxygens (b). (c) and (d) Computed ODFs of water around phosphate group (c) and carbonyl group (d). The second peak, around 90°–120° in both plots, corresponds to the H atom that is not directly hydrogen-bonded to the phosphate or carbonyl group.

in both lipids are nearly identical [Fig. 3(a)]. However, the RDF of the carbonyl-associated water around DOCPe shows a slightly smoother shape than that around DOPC lipid carbonyl groups, particularly around the second solvation shell [0.4–0.6 nm, Fig. 3(b)]. This implies that (1) the carbonyl-associated water H-bond structure in the DOCPe lipid bilayer system is more disordered compared to DOPC, especially at the second hydration shell. This is consistent with the H-bond populations [Fig. 1(d)], which shows the reduced H-bond number for DOCPe. (2) Such disordered H-bond structures are only represented in the linker region but not in the phosphate region, suggesting that there is a subtle perturbation by the inverted-headgroups (i.e., the electric field generated between the phosphate and the choline groups), which is not observed in the headgroup region.

The RDFs of water around choline groups were also computed using the nitrogen atom as a reference (Fig. S4). The RDFs of choline-associated water in both lipids show slight differences. In the DOCPe system, the choline-associated water has slightly less defined solvation shell peaks compared to DOPC, suggesting an increased disorder in the water structure around this group. In addition, the second solvation shell is shifted, likely a result of the different headgroup structures.

Phosphate- and carbonyl-associated water ODFs are shown in Figs. 3(c) and 3(d), respectively. Here, we used the following definitions: (1) Distances between donor oxygen and acceptor oxygen is less than the first minimum positions in RDFs [<0.31 nm, Figs. 3(a) and 3(b)] and (2) angles are defined as the angle between the water O–H vector and vector connecting the carbonyl/phosphate oxygen (i.e., acceptor) and water oxygen (i.e., donor). Both carbonyl and phosphate ODFs are indistinguishable for both lipids, suggesting that the inverted-headgroup effect on the first hydration shell is minor and, therefore, explaining the underlying reason why the carbonyl dynamics in both lipid systems are almost identical.

D. Interfacial water dynamics

The H-bond structure of both DOPC and DOCPe is very similar despite the differences in dipole orientations. A further view of water dynamics can be obtained through lateral (xy plane) and orientational diffusion plots. The water mean-squared displacements (MSDs) are shown in Fig. 4(a). The plots show nearly identical dynamics. Self-diffusion coefficients in both systems are identical within error ($1.94 \pm 0.12 \times 10^{-5}$ cm^2/s for DOPC system and $1.97 \pm 0.09 \times 10^{-5}$ cm^2/s for DOCPe system), meaning that the inverted-headgroup orientation does not affect the overall translational properties of water. A similar analysis is performed for the interfacial water (Fig. S5), also showing nearly identical diffusion rates across both lipid species; however, slightly faster diffusion rates of the interfacial water for the DOCPe system than for the DOPC system may be a result of the larger area-per-lipid of DOCPe.

Orientational relaxation functions of water in both systems also showed the almost identical orientational dynamics [Fig. 4(b)].

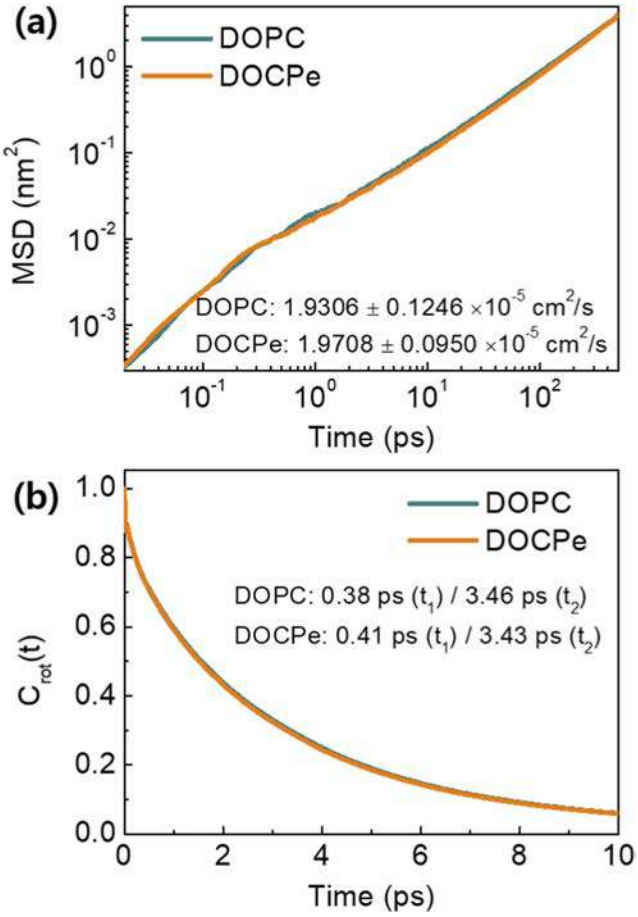

FIG. 4. (a) Mean-squared displacements (MSDs) of water molecules in simulation. (b) Orientational relaxation functions of whole water molecules in simulation boxes and their time constants obtained from the bi-exponential decay function.

Here, the orientational relaxation function[49–52] is defined as

$$C_{rot}(t) = \langle P_2(\hat{u}_{\mathrm{OH}}(t) \cdot \hat{u}_{\mathrm{OH}}(0)) \rangle, \quad (1)$$

where $P_2(x)$ is the second-order Legendre polynomial function, and $\hat{u}_{\mathrm{OH}}(t)$ is the O–H unit vector. The relaxation can be described by a biexponential decay pattern with time constants of 0.38 and 3.46 ps for DOPC lipid bilayer systems and 0.41 and 3.43 ps for DOCPe, respectively.

IV. DISCUSSION

Analysis of the H-bond structure and dynamics from the present experiments and simulations are consistent with previous sum frequency generation (SFG) spectroscopy studies of Deiseroth *et al.*[25] We found out that the inverted-headgroup and its interfacial water have negligible effects on interfacial water properties, but they slightly perturb the local H-bond structure at the linker region between the headgroup and the lipid tail. This indicates that water dynamics are largely driven by short-range interactions with the polar headgroup phosphate and the choline but not on the global orientation at the interface. In other words, since both DOPC and DOCPe have the same phosphate and choline groups, which produce nearly identical dynamics. Other studies have indicated that interfacial dynamics are largely dependent on the headgroup structure, especially the phosphate group.[14,16] Therefore, the present studies indicate that although the net water orientation may be modulated by the local electric fields, the H-bond structure and dynamics are only dependent on the local headgroup composition and overall lipid–lipid interactions that determine packing.

Finally, despite the minor effects on interfacial H-bonds, the large dipole induced by the headgroup could significantly modulate the structure and orientation of membrane proteins. Inverted-headgroup lipids are an excellent experimental platform to further test any effects, or lack thereof, on the structure or the function of transmembrane proteins.

V. CONCLUSIONS

Here, we investigated the interfacial H-bond structure and dynamics of the DOPC and DOCPe lipid bilayers using 2D IR spectroscopy and MD simulations, particularly focusing on the carbonyl-associated water located near the linker region. We found that the inverted-headgroup has only a minor effect on the carbonyl dynamics and its H-bonding properties, which is the partially disrupted H-bond between the carbonyl group and water. Simulations also showed the negligible effect of the inverted-headgroup on the carbonyl dynamics and the interfacial water H-bond structure and dynamics. Interestingly, a subtle perturbation was observed near the linker region, especially within the second hydration shell that could reflect slight changes in lipid packing or other long-range interactions. These results add to the recent literature focused on understanding the dipole effects on water orientation.[24] These studies answer the question of whether the headgroup dipole orientation perturbs interfacial H-bonds, but there is still an important question of the extent to which headgroup electrostatics affect the protein structure, orientation, or function within more complex cell membranes.

SUPPLEMENTARY MATERIAL

Structural information of the lipid bilayers, chemical structure of DOPC and DOCPe lipids for DFT calculations, area-per-lipids of DOPC lipid bilayers and FFCF decay constants with different lateral pressures, RDFs of choline-associated water, computed self-diffusion coefficients, and rotational relaxation decay time constants of interfacial/bulk water are included in the supplementary material.

ACKNOWLEDGMENTS

This work was supported by the National Institutes of Health (Grant No. R35GM133359) and the Welch Foundation (Grant No. F-1891). Molecular dynamics simulations using the computing facilities at the Texas Advanced Computing Center (TACC).

AUTHOR DECLARATIONS

Conflict of Interest

The authors have no conflicts to disclose.

DATA AVAILABILITY

The data that support the findings of this study are available from the corresponding author upon reasonable request.

REFERENCES

[1]W. Dowhan and M. Bogdanov, Annu. Rev. Biochem. **78**, 515–540 (2009).
[2]G. von Heijne, J. Mol. Biol. **225**(2), 487–494 (1992).
[3]C. H. Hsieh and W. G. Wu, Biophys. J. **71**(6), 3278–3287 (1996).
[4]D. F. Bocian and S. I. Chan, Annu. Rev. Phys. Chem. **29**, 307–335 (1978).
[5]T. Adachi, H. Takahashi, K. Ohki, and I. Hatta, Biophys. J. **68**(5), 1850–1855 (1995).
[6]S. Tristram-Nagle and J. F. Nagle, Chem. Phys. Lipids **127**(1), 3–14 (2004).
[7]K. Gawrisch, H. C. Gaede, M. Mihailescu, and S. H. White, Eur. Biophys. J. **36**(4–5), 281–291 (2007).
[8]N. Kucerka, J. F. Nagle, J. N. Sachs, S. E. Feller, J. Pencer, A. Jackson, and J. Katsaras, Biophys. J. **95**(5), 2356–2367 (2008).
[9]K. J. Tielrooij, D. Paparo, L. Piatkowski, H. J. Bakker, and M. Bonn, Biophys. J. **97**(9), 2484–2492 (2009).
[10]S. E. Feller, Curr. Opin. Colloid Interface Sci. **5**, 217–223 (2000).
[11]P. B. Moore, C. F. Lopez, and M. L. Klein, Biophys. J. **81**(5), 2484–2494 (2001).
[12]S. M. Gruenbaum and J. L. Skinner, J. Chem. Phys. **135**(7), 075101 (2011).
[13]S. Re, W. Nishima, T. Tahara, and Y. Sugita, J. Phys. Chem. Lett. **5**(24), 4343–4348 (2014).
[14]E. Lee, A. Kundu, J. Jeon, and M. Cho, J. Chem. Phys. **151**(11), 114705 (2019).
[15]W. Zhao, D. E. Moilanen, E. E. Fenn, and M. D. Fayer, J. Am. Chem. Soc. **130**(42), 13927–13937 (2008).
[16]A. Kundu, K. Kwak, and M. Cho, J. Phys. Chem. B **120**(22), 5002–5007 (2016).
[17]A. Kundu, B. Błasiak, J.-H. Lim, K. Kwak, and M. Cho, J. Phys. Chem. Lett. **7**(5), 741–745 (2016).
[18]R. K. Venkatraman and C. R. Baiz, Langmuir **36**(23), 6502–6511 (2020).
[19]M. L. Valentine, M. K. Waterland, A. Fathizadeh, R. Elber, and C. R. Baiz, J. Phys. Chem. B **125**(5), 1343–1350 (2021).
[20]N. Ji, V. Ostroverkhov, C.-Y. Chen, and Y.-R. Shen, J. Am. Chem. Soc. **129**(33), 10056–10057 (2007).
[21]T. Ohto, E. H. G. Backus, C.-S. Hsieh, M. Sulpizi, M. Bonn, and Y. Nagata, J. Phys. Chem. Lett. **6**(22), 4499–4503 (2015).
[22]J. A. Mondal, S. Nihonyanagi, S. Yamaguchi, and T. Tahara, J. Am. Chem. Soc. **132**(31), 10656–10657 (2010).
[23]J. A. Mondal, S. Nihonyanagi, S. Yamaguchi, and T. Tahara, J. Am. Chem. Soc. **134**(18), 7842–7850 (2012).
[24]L. B. Dreier, A. Wolde-Kidan, D. J. Bonthuis, R. R. Netz, E. H. G. Backus, and M. Bonn, J. Phys. Chem. Lett. **10**(20), 6355–6359 (2019).
[25]M. Deiseroth, M. Bonn, and E. H. G. Backus, Phys. Chem. Chem. Phys. **22**(18), 10142–10148 (2020).
[26]T. Starke-Peterkovic and R. J. Clarke, Eur. Biophys. J. **39**(1), 103–110 (2009).
[27]X. Chen, W. Hua, Z. Huang, and H. C. Allen, J. Am. Chem. Soc. **132**(32), 11336–11342 (2010).
[28]E. K. Perttu, A. G. Kohli, and F. C. Szoka, Jr., J. Am. Chem. Soc. **134**(10), 4485–4488 (2012).
[29]R. J. Clarke, Biochim. Biophys. Acta **1327**(2), 269–278 (1997).
[30]X. You, E. Lee, C. Xu, and C. R. Baiz, J. Phys. Chem. Lett. **12**, 9602–9607 (2021).
[31]S. C. Edington, A. Gonzalez, T. R. Middendorf, D. B. Halling, R. W. Aldrich, and C. R. Baiz, Proc. Natl. Acad. Sci. U. S. A. **115**(14), E3126–E3134 (2018).
[32]Q. Guo, P. Pagano, Y.-L. Li, A. Kohen, and C. M. Cheatum, J. Chem. Phys. **142**(21), 212427 (2015).
[33]H. J. C. Berendsen, D. Vanderspoel, and R. Vandrunen, Comput. Phys. Commun. **91**(1–3), 43–56 (1995).
[34]J. B. Klauda, R. M. Venable, J. A. Freites, J. W. O'Connor, D. J. Tobias, C. Mondragon-Ramirez, I. Vorobyov, A. D. MacKerell, Jr., and R. W. Pastor, J. Phys. Chem. B **114**(23), 7830–7843 (2010).
[35]S. Jo, T. Kim, V. G. Iyer, and W. Im, J. Comput. Chem. **29**(11), 1859–1865 (2008).
[36]E. L. Wu, X. Cheng, S. Jo, H. Rui, K. C. Song, E. M. Dávila-Contreras, Y. Qi, J. Lee, V. Monje-Galvan, R. M. Venable, J. B. Klauda, and W. Im, J. Comput. Chem. **35**(27), 1997–2004 (2014).
[37]S. Jo, J. B. Lim, J. B. Klauda, and W. Im, Biophys. J. **97**(1), 50–58 (2009).
[38]S. Jo, T. Kim, and W. Im, PLoS One **2**(9), e880 (2007).
[39]L. Martínez, R. Andrade, E. G. Birgin, and J. M. Martínez, J. Comput. Chem. **30**(13), 2157–2164 (2009).
[40]H. W. Horn, W. C. Swope, J. W. Pitera, J. D. Madura, T. J. Dick, G. L. Hura, and T. Head-Gordon, J. Chem. Phys. **120**(20), 9665–9678 (2004).
[41]T. Darden, D. York, and L. Pedersen, J. Chem. Phys. **98**(12), 10089–10092 (1993).
[42]D. van der Spoel, P. J. van Maaren, P. Larsson, and N. Tîmneanu, J. Phys. Chem. B **110**(9), 4393–4398 (2006).
[43]M. J. Abraham, T. Murtola, R. Schulz, S. Páll, J. C. Smith, B. Hess, and E. Lindahl, SoftwareX **1–2**, 19–25 (2015).
[44]S. C. Edington, J. C. Flanagan, and C. R. Baiz, J. Phys. Chem. A **120**(22), 3888–3896 (2016).
[45]M. J. Frisch, G. W. Trucks, H. B. Schlegel, G. E. Scuseria, M. A. Robb, J. R. Cheeseman, G. Scalmani, V. Barone, G. A. Petersson, H. Nakatsuji, X. Li, M. Caricato, A. V. Marenich, J. Bloino, B. G. Janesko, R. Gomperts, B. Mennucci, H. P. Hratchian, J. V. Ortiz, A. F. Izmaylov, J. L. Sonnenberg, D. Williams-Young, F. Ding, F. Lipparini, F. Egidi, J. Goings, B. Peng, A. Petrone, T. Henderson, D. Ranasinghe, V. G. Zakrzewski, J. Gao, N. Rega, G. Zheng, W. Liang, M. Hada, M. Ehara, K. Toyota, R. Fukuda, J. Hasegawa, M. Ishida, T. Nakajima, Y. Honda, O. Kitao, H. Nakai, T. Vreven, K. Throssell, J. A. Montgomery, Jr., J. E. Peralta, F. Ogliaro, M. J. Bearpark, J. J. Heyd, E. N. Brothers, K. N. Kudin, V. N. Staroverov, T. A. Keith, R. Kobayashi, J. Normand, K. Raghavachari, A. P. Rendell, J. C. Burant, S. S. Iyengar, J. Tomasi, M. Cossi, J. M. Millam, M. Klene, C. Adamo, R. Cammi, J. W. Ochterski, R. L. Martin, K. Morokuma, O. Farkas, J. B. Foresman, and D. J. Fox, Gaussian 16, Revision B.01, Gaussian, Inc., Wallingford, CT, 2016.
[46]A. P. Scott and L. Radom, J. Phys. Chem. **100**(41), 16502–16513 (1996).
[47]J.-H. Choi and M. Cho, J. Chem. Phys. **134**(15), 154513 (2011).
[48]J. C. Flanagan, M. L. Valentine, and C. R. Baiz, Acc. Chem. Res. **53**(9), 1860–1868 (2020).
[49]Y.-l. Yeh and C.-Y. Mou, J. Phys. Chem. B **103**(18), 3699–3705 (1999).
[50]J. Ropp, C. Lawrence, T. C. Farrar, and J. L. Skinner, J. Am. Chem. Soc. **123**(33), 8047–8052 (2001).
[51]E. J. W. Wensink, A. C. Hoffmann, P. J. van Maaren, and D. van der Spoel, J. Chem. Phys. **119**(14), 7308–7317 (2003).
[52]D. Laage, G. Stirnemann, F. Sterpone, R. Rey, and J. T. Hynes, Annu. Rev. Phys. Chem. **62**, 395–416 (2011).